Lawrence Berkeley National Laboratory
LBL Publications

Title

Coupled geomechanics and flow modeling of thermally induced compaction in heavy oil diatomite reservoirs under cyclic steaming

Permalink

https://escholarship.org/uc/item/16g9m7w8

Authors

Blanco-Martín, Laura
Rutqvist, Jonny
Doughty, Christine
et al.

Publication Date

2016-11-01

DOI

10.1016/j.petrol.2016.09.002

Peer reviewed

eScholarship.org Powered by the California Digital Library
University of California

Coupled geomechanics and flow modeling of thermally induced compaction in heavy oil diatomite reservoirs under cyclic steaming

Author links open overlay panelLauraBlanco-MartínJonnyRutqvistChristineDoughtyYingqiZhangStefanFinsterleCurtis M.Oldenburg
Show more

https://doi.org/10.1016/j.petrol.2016.09.002Get rights and content

Highlights

- Coupled modeling of enhanced heavy oil recovery from diatomite using cyclic steaming.
- Increasing temperature weakens diatomite rock and enhances reservoir compaction.
- Non-recoverable thermally-induced compaction of diatomite intensifies subsidence.
- Modified Cam-clay model with temperature-dependent cap.
- Thermally-induced compaction may play an important role in well failure.

Abstract

Shallow, heavy oil diatomite reservoirs produced using cyclic steaming are often associated with significant subsidence. In cases where the pore pressure is not allowed to deplete noticeably, observed subsidence suggests a mechanism other than pressure decline is responsible. We perform coupled flow and geomechanics modeling to determine whether thermally induced compaction of the reservoir rockcould play an important role in subsidence. First, we model laboratory-scale tests on diatomite samples subjected to mechanical and thermal loads. During these tests, substantial non-recoverable thermal compaction was measured. Using the modified Cam-clay

model as a basis, thermally induced compaction is implemented by reducing the size of the yield surface as a function of temperature. This leads to a satisfactory modeling of the test results. Second, this new approach is used to model a symmetric pattern of wells in a generic heavy oil diatomite field produced using cyclic steaming. Results from simulations that consider or neglect thermally induced diatomite compaction show that thermal effects can potentially induce significant inelastic pore volume reduction and substantial subsidence.

Keywords

Diatomite
Heavy oil
Cyclic steaming
Thermally induced compaction
Ground displacement
Coupled modeling

1. Introduction

Diatomite is a unique rock that results from the fossilization of the rigid silica shells of diatoms, which are single-celled micro-organisms living in fresh and salt waters, and whose shells have accumulated to create thick layers that were buried and subsequently fossilized. Regular inter-granular porosities, combined with high internal void spaces (due to the hollow shells that remain once diatoms die), result in the atypically high porosities (45–70%) characteristic of diatomaceous rocks. In addition, diatomite is quite compressible and features fine grain sizes, small pore-throat diameters and undisturbed permeabilities on the order of $5{\cdot}10^{-16}$–10^{-14} m^2(0.5–10 md) (Crawford et al., 2006, Kumar and Beatty, 1995). Owing to its high storativity and low permeability, diatomites serve as hydrocarbon reservoirs(Crawford et al., 2006, Hascakir and Kovscek, 2010). The San Joaquin Valley in central California has well-documented examples of diatomite reservoirs, with billions of barrels of original oil in place (Dietrich, 2010, Fredrich et al., 2000, Ilderton et al., 1994, Kumar and Beatty, 1995).

This research focuses on shallow, heavy oil diatomite reservoirs produced using cyclic steaming. Cyclic steaming is an enhanced oil recovery method that consists of the injection of steam into the reservoir for a few days, followed by a soaking period (i.e., the well is shut in), and a final phase of production through the same well (“huff and puff” recovery method). The high enthalpy of the injected steam heats the surrounding

oil and reduces its viscosity, allowing the oil to flow to the well during the production phase. The injection-soak-production pattern is repeated over time as long as operations are profitable. Cyclic steaming is an alternative to steam flooding when the permeability of the reservoir is too low to allow connectivity between injectors and producers, or when the viscosity of the oil is too high to allow significant hydrocarbon mobilization between different wells. It may also be used to improve injectivity prior to steam flooding operations (Hascakir and Kovscek, 2010).

In spite of the beneficial effect of heating on viscosity reduction, laboratory experiments and field observations show that there is a mechanical drawback to thermal stimulation of diatomite reservoirs: as temperature increases, silica dissolution/precipitation, reordering and mineralogical transformations of amorphous silica (Opal-A) into more structured and dense phases (such as Opal-CT and quartz) result in significant non-recoverable thermal compaction, triggering a reduction in porosity, permeability, and mechanical integrity of the reservoir rock(Crawford et al., 2006, Dietrich and Scott, 2007, Koh et al., 1996). Thus, as the reservoir is heated up, there is a strong interplay between thermal, hydraulic, chemical and mechanical processes that leads to diatomite weakening and to inelastic reservoir pore volume reduction.

At a larger scale, reservoir compaction may induce surface subsidence, as well as differential movements within the overburden — in particular at the flanks of the reservoir, and/or at possible weak layers present in the overburden with contrasting mechanical properties. Horizontal movements within the overburden, if large enough, can cause well shear failure. In the San Joaquin Valley, thousands of wells have been reported to fail since the 1990s due to lateral shearing induced by subsidence (Bruno, 1990, Hamilton et al., 1992, Hilbert et al., 1996, Fredrich et al., 2000, Yudovich and Morgan, 1989).

In this paper, our main goal is to quantify the impacts of thermally induced diatomite compaction on reservoir behavior and induced ground surface movements. For this purpose, we have developed a mechanistic model that reproduces thermal weakening observed in laboratory-scale tests performed on several types of diatomite rock (tests conducted by Dietrich and Scott (2007)), and we have subsequently used that mechanistic model to study a symmetric pattern of wells in a generic heavy oil diatomite reservoir, focusing particularly on local effects around wells (e.g., heat propagation, phase transitions, changes in pore pressure, oil displacement, reservoir rock yield, porosity variations). Previous investigations regarding thermal recovery (not cyclic steaming) from heavy oil diatomite reservoirs used pressure depletion as the key

driving factor for reservoir compaction, subsidence and well failure, without addressing the effect of temperature on the mechanical response of the reservoir rock (DeRouffignac et al., 1995, Fredrich et al., 2000, Fredrich et al., 1996, Hansen et al., 1995, Hilbert et al., 1999, Minkoff et al., 2004). However, in cases where the reservoir pore pressure is not allowed to deplete noticeably (as it often occurs in cyclic steaming), another mechanism must be responsible for reservoir compaction, related subsidence and massive well failure. In this study, we investigate whether thermal effects on the mechanical behavior of diatomite could be important, and in particular the degree to which thermal effects may contribute to compaction and associated subsidence.
Previous modeling studies about cyclic steaming of diatomite reservoirs focused on the optimization of operations and on the improvement of reservoir management, without considering coupled thermal-hydraulic-mechanical (THM) processes, and therefore without addressing the mechanical response of the reservoir rock (Ambastha et al., 2001, Fong et al., 2001, Kumar and Beatty, 1995).
This paper is organized as follows. First, we present the approach selected to model observed thermally induced compaction of diatomite. This approach is based on the use of the modified Cam-clay model (Roscoe and Burland, 1968, Wood, 1991), and its particularity consists in making the cap size (i.e., the size of the yield surface) stress and temperature dependent (in the classical model, no temperature dependence is considered). The parameters that define the temperature dependence of the cap size are calibrated against data from laboratory tests in which diatomite samples were subjected to stress and temperature loads (Dietrich and Scott, 2007). Then, we describe briefly iTOUGH2-FLAC, the simulator used to model two-way, sequentially coupled flow and geomechanics processes (THM). Using iTOUGH2-FLAC and the approach described to model thermally induced compaction, we simulate a symmetric pattern of wells in a generic heavy oil diatomite reservoir undergoing cyclic steaming. In order to examine how much thermal effects influence the mechanical response of the reservoir rock and induced ground surface displacement, we compare results from two THM simulations that use, respectively, the standard or the temperature-enhanced modified Cam-clay model. From the comparison, we conclude that thermally induced diatomite compaction can trigger significant inelastic pore volume reduction and substantial subsidence. This finding, linked with differential movements in the overburden, shows that thermally induced compaction is most likely an important mechanism for massive well shear failure at the field scale.

2. Materials and methods

2.1. Modified Cam-clay model with temperature-dependent cap

Dietrich and Scott (2007) performed a series of tests on diatomite samples having different mineralogical compositions (ranging from Opal-A to Opal-CT). Initial porosities of the samples were between 50% and 70%. The test conditions were similar to those of a constrained thermal test in an oedometer. In the context of our research, we have analyzed several tests presented in Dietrich and Scott (2007). Of particular interest to us are the tests in which first a mechanical load was applied stepwise to a sample at ambient temperature (22 °C [72 °F]), and then the load was kept constant (different loading levels for different samples) and the temperature was increased progressively to 288 °C (550 °F). The samples were flushed and saturated with toluene or water. According to Dietrich and Scott (2007), four significant findings from these tests were that (i) the strains induced during the heating phase were comparable to the strains induced during the mechanical loading phase, (ii) for all tests, the effect of temperature on the strain was more pronounced for T<102 °C (215 °F), (iii) the initial stress level affected the strains during the thermal loading, and (iv) for a given stress level, steam-saturated samples were less compressible than toluene-saturated samples (the rock is apparently stronger when it is saturated with steam). Moreover, during the thermal unloading phase (at constant stress), no significant recovery of the strain induced during the heating phase was measured. Putting off for now the explanation of the lines in Fig. 1, the symbols represent experimental data relative to several stress (Fig. 1a) and temperature (Fig. 1b) stages presented in Dietrich and Scott (2007). Only the loading stages of the tests are shown. The development of the model used to generate the results shown by the lines in Fig. 1 will be discussed below.

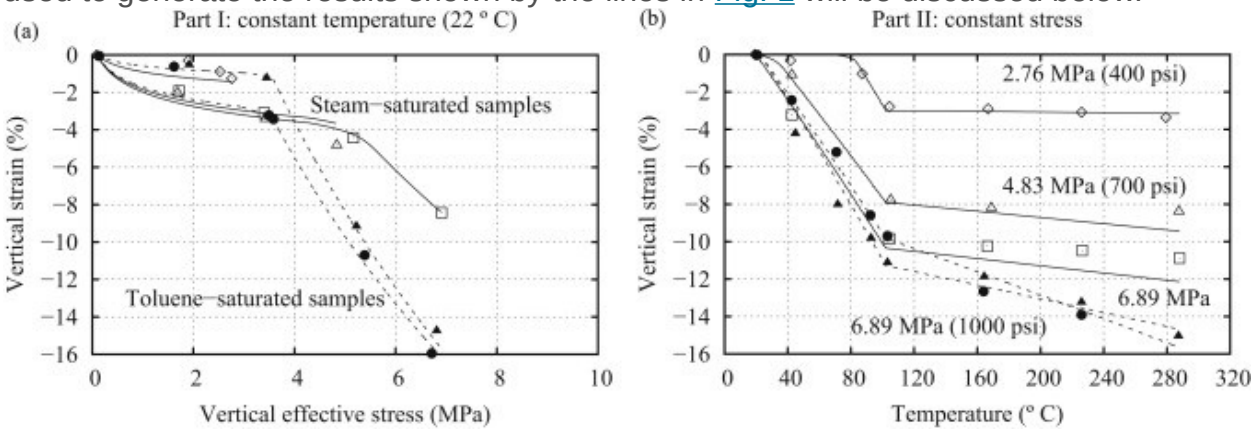

1. Download high-res image (405KB)
2. Download full-size image

Fig. 1. Comparison between experimental data (symbols) and modeling results (lines) for laboratory-scale tests on diatomite samples (data from Dietrich and Scott (2007)): (a)

loading at constant temperature; (b) heating at constant stress. Modeling results include thermally induced compaction. Solid lines correspond to steam-saturated samples and dashed lines correspond to toluene-saturated samples.

Given the significant amount of non-reversible volume reduction measured during the thermal loading, the proper modeling of these tests requires that not only mechanical, but also thermal compaction of diatomite be considered.

Non-recoverable compaction is modeled using a constitutive relationship that considers failure due to an excess of hydrostatic (or mean) stress. Here, we focus on cap models, which account for both shear and hydrostatic failure. A detailed description of some cap models (such as Cam-clay and Granta-gravel) can be found in Schofield and Wroth (1968). Another example of a cap model is the modified Cam-clay model (Roscoe and Burland, 1968, Wood, 1991). The main difference between the Cam-clay and the modified Cam-clay models is the form of the yield surface.

In this study, we have used the modified Cam-clay model as a basis, and we have introduced a temperature dependence of failure to account for the processes observed experimentally in heated diatomite. The modified Cam-clay model is available in FLAC^{3D} (Itasca, 2012). In this model, the failure envelope (or cap) is an ellipse in the von Mises equivalent stress (q) vs. mean effective stress (p) plane. The flow rule is associated and the yield function $F=0$ is given by

$$F(p,q)=q^2+M^2p(p-p_c) \quad (1)$$

Eq. (1) defines an ellipse with center ($p_c/2$,0) and maximum vertex along the $p$axis equal to p_c. Parameter M represents the ratio of the semi axes along q and p, and corresponds to the slope of the critical state line $q=M\,p$ (straight line intersecting the ellipse at the critical point ($p_c/2$, $M\,p_c/2$)). The consolidationpressure, p_c, is defined as the mean effective stress at which yielding occurs in hydrostatic conditions (q=0). Thus, the consolidation pressure defines the size of the yield envelope along the p axis. Compression is considered positive here. Upon failure, the consolidation pressure can either increase (hardening and associated plastic compaction, domain $p>p_c/2$), decrease (softening and associated plastic dilation, domain $p<p_c/2$) or remain constant ($p=p_c/2$, no change in plastic volumetric deformation and unlimited shear failure without change in volume [critical point]). Therefore, the failure surface is defined by a series of ellipses in the (p,υ,q) space, where υ is the specific volume, defined as

$$\upsilon=\frac{V}{V_s}=\frac{1}{1-\phi}=1+e \quad (2)$$

In Eq. (2), V is the total volume, $V_s=V-V_p$ is the volume of the non-porous (solid) space (V_p is the pore volume), ϕ is porosity and e is the void ratio (υ, ϕ and e are dimensionless). Fig. 2 shows the failure surface of the modified Cam-clay model.

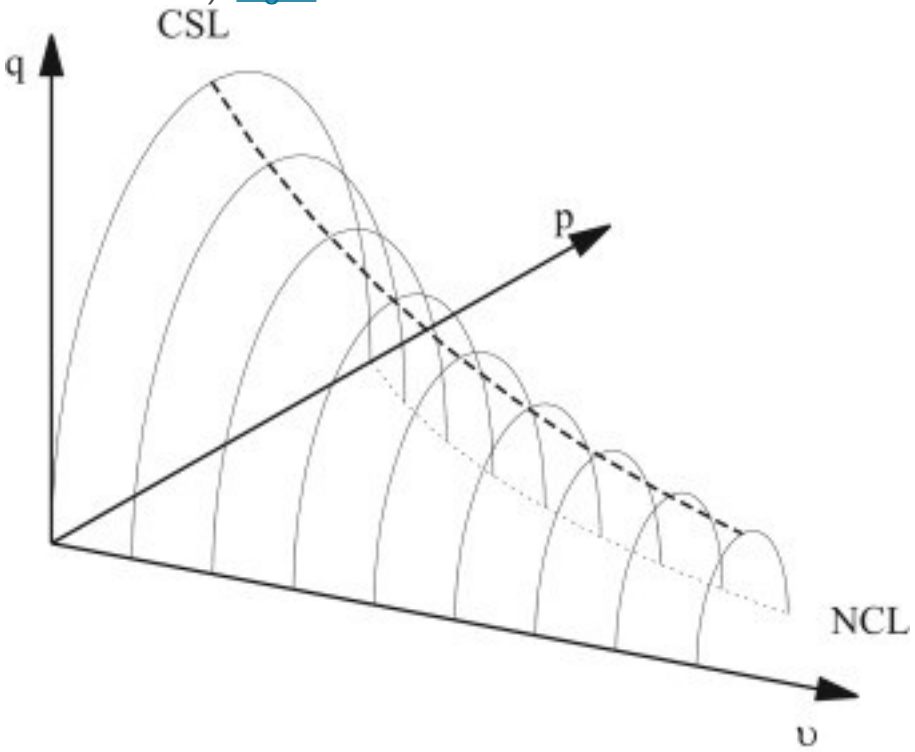

1. Download high-res image (133KB)
2. Download full-size image

Fig. 2. Schematic yield surface of the modified Cam-clay model in the (p,υ,q) space. The critical state line ("CSL", dashed line) and the normal consolidation line ("NCL", dotted line) are also shown.

Specific volume and volumetric strain are related according to (recall that compression is positive in the derivation here)

(3)$\varepsilon_{ll}=-d\upsilon$

Changes in the consolidation pressure follow

(4)$p_{cnew}=p_c(1+\varepsilon_{llpl}\upsilon\lambda-\kappa)$

where ε_{llpl} is the incremental plastic volumetric strain (i.e., inelastic compaction or dilation), p_c is the current consolidation pressure, and κ and λ are material parameters, corresponding, respectively, to the slopes of the swelling lines and the normal consolidation line, defined in hydrostatic conditions (Itasca Consulting Group, 2012, Roscoe and Burland, 1968). These parameters represent dimensionless compressibility in elasticity and plasticity, respectively. The swelling and normal consolidation lines can be expressed, respectively, as

(5)υ=υκ−κln(pp1)

(6)υ=υλ−λln(pp1)

where p_1 is a reference pressure and υ_κ and υ_λ are the specific volumes corresponding to p_1 on each of the lines. These lines are shown in Fig. 3 (ln(p)−υplane). Note that the normal consolidation line defines admissible (υ,p_c) (or (υ, ln(p_c))) pairs (see Fig. 2), and that an infinite number of swelling lines can be defined depending on the stress path (loading/unloading). Given the non-linear relationship between p and υ defined in Eq. (5), the tangent bulk modulus is not constant (non-linear elasticity), but evolves following

(7)K=υpκ

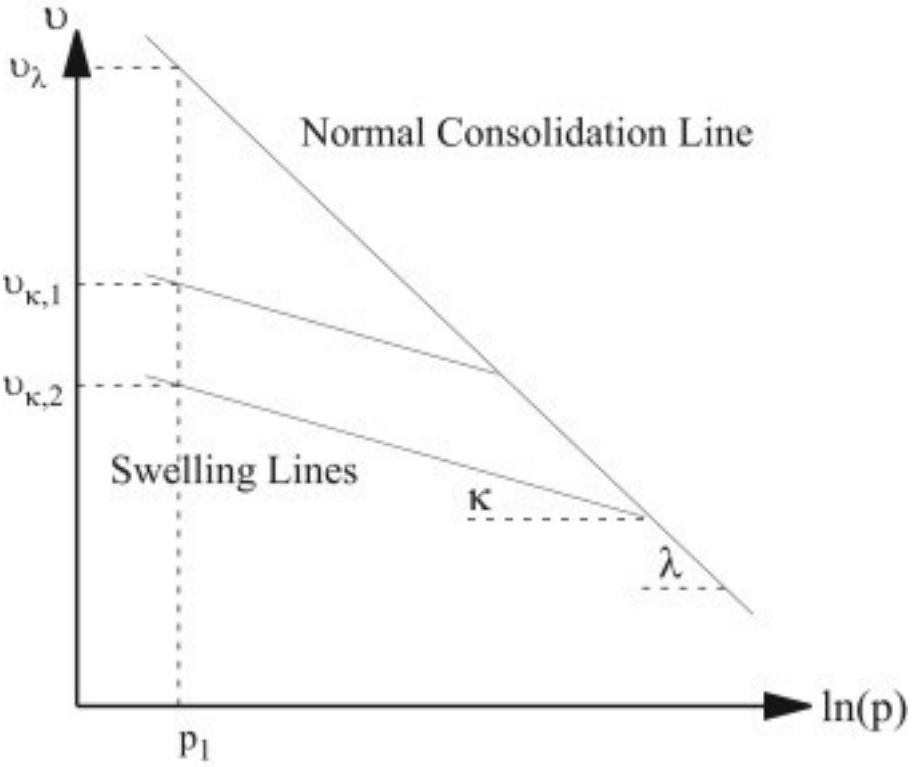

1. Download high-res image (115KB)
2. Download full-size image

Fig. 3. Normal consolidation line and two swelling lines in the ln(p)−υ plane (modified Cam-clay model).

In order to include thermal weakening, we have added two provisions into the modified Cam-clay model. First, parameter λ decreases linearly with an increase in temperature. Reducing λ as temperature increases is also the approach selected previously by Crawford et al. (2006) to model hydrostatic tests on diatomite samples. According to experimental observations (Fig. 1b), the temperature effect on λ reduction is stronger

for T<102 °C. For T<102 °C, the relationship found to best match experimental data reads

(8)λ(T)=0.45−0.00139·(T−20).

with T [°C]. For T>102 °C, it reads (also with T [°C])

(9)λ(T)=0.33611−0.0001·(T−102)

Eqs. (8), (9) have been calibrated from steam-saturated samples (more relevant with a view to cyclic steaming of an oil field). Note, however, that the relationships found for toluene-saturated samples are similar. Additionally, for typical values of κon the order of 0.01, these equations verify that $\lambda(T)>\kappa$, $\forall\ T\in$ [20,300] °C (relevant temperature range). Second, and due to the reduction in λ, the consolidation pressure changes. The intersection between the original and temperature-modified normal consolidation lines is kept constant at a point calibrated from experimental data. For steam-saturated samples with initial porosity around 68–70% ($v_0\approx3-3.3$) (conditions very close to the generic diatomite oil field investigated in the next section), the intersection point is at (p_i,v_i)=(64.4 MPa,1.7). Since $v_0>v_i$, the consolidation pressure (defined on a new temperature-modified normal consolidation line) decreases as λ decreases.

Using these provisions, as temperature increases the size of the cap decreases and the elastic domain shrinks, thereby decreasing the threshold for non-reversible behavior. In the plastic compaction domain ($p>p_c/2$), this results in additional non-recoverable volume reduction.

The lines in Fig. 1 correspond to modeling results using the modified Cam-clay model with a temperature-dependent cap. Overall, experimental data and numerical results match closely (note that some parameters such as the initial consolidation pressure vary among the samples). Fig. 4 illustrates some ellipses in the p–q plane, including the temperature dependence of the consolidation pressure. As the figure shows, the effect of temperature on the cap size is much more important below 102 °C.

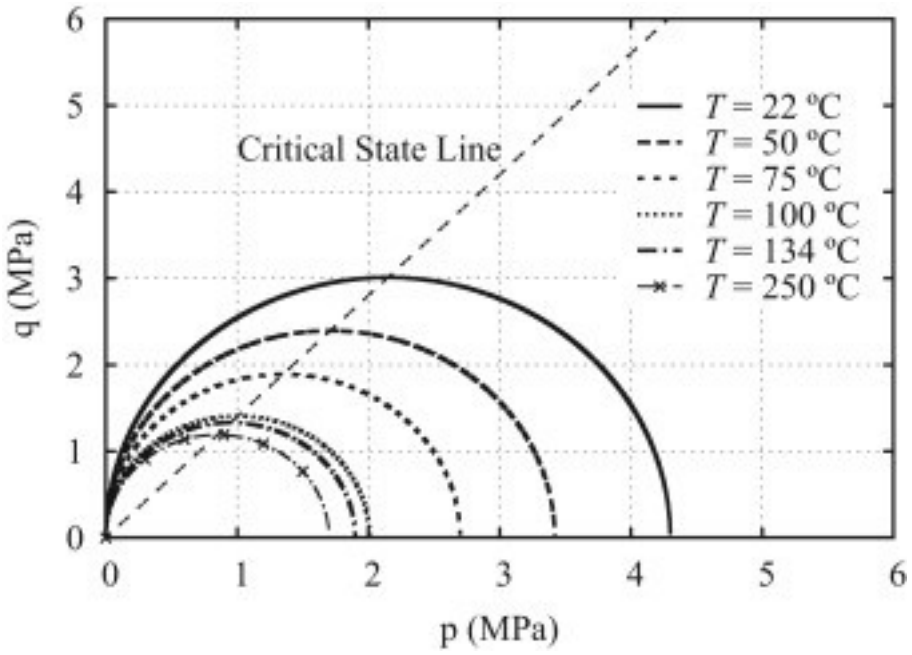

1. Download high-res image (194KB)
2. Download full-size image

Fig. 4. Modified Cam-clay model with temperature-dependent cap: view of some ellipses in the *p*–*q* plane, including projection of the critical state line.

Finally, it should be noted that the approach presented to model thermal weakening of diatomite accounts for a structural transformation of the rock under increasing temperature, but it does not explicitly consider processes such as mineralogical transformations or mass changes that could arise from silicadissolution/precipitation; the overall behavior is parameterized to fit the observed macroscopic response.

2.2. iTOUGH2-FLAC with temperature-dependent cap model and dead-oil equation of state module

In order to study two-way coupled flow and geomechanics processes related to cyclic steaming in a heavy oil diatomite reservoir, we use the iTOUGH2-FLAC simulator (Blanco-Martín et al., 2015). iTOUGH2-FLAC has been recently developed based on TOUGH-FLAC (Rutqvist, 2011, Rutqvist et al., 2002), a well-established simulator for two-way coupled flow and geomechanics processes. In these simulators, the flow and geomechanics equations are solved sequentially within a time step (i.e., one system of equations after the other [geomechanics after flow]), and relevant information (such as volumetric strain, pore pressure and temperature) is passed between the two systems of equations through a THM interface (details can be found in Rutqvist (2011)). The two simulators use FLAC^{3D}(Itasca, 2012) to solve the geomechanics sub-problem.

Regarding the flow sub-problem, TOUGH-FLAC uses TOUGH2 (Pruess et al., 2012), and iTOUGH2-FLAC uses iTOUGH2 (Finsterle et al., 2016, Finsterle, 2004). Both programs solve non-isothermal, multi-phase and multi-component fluid flow in porous and fractured media. Additionally, iTOUGH2 provides inverse modeling capabilities for TOUGH2 (including parameter estimation, sensitivity analysis, uncertainty propagation and data-worth analysis). The motivations to develop iTOUGH2-FLAC were mainly (i) to take advantage of the enhancements implemented in iTOUGH2 relative to standard TOUGH2 to run a forward model (Finsterle, 2015), and (ii) to be able to use the inverse modeling capabilities of iTOUGH2 on a model response that accounts for geomechanical effects. An example of an enhancement implemented in iTOUGH2 is that this code allows changing boundary conditions and flow properties in different elements during a simulation, without the need to stop and restart (in the current case, a significant number of cycles is modeled, which would have required multiple restarts using standard TOUGH2). Finally, we note that iTOUGH2 supports the PEST protocol (Doherty, 2008), through which the inverse modeling capabilities of iTOUGH2 can be applied to the analysis of any user-supplied model — such as a coupled flow and geomechanics model. This way, it is possible to perform inversions on flow and/or mechanical parameters (Finsterle and Zhang, 2011).

As for the geomechanics sub-problem, the main innovation is the use of the modified Cam-clay model with a temperature-dependent cap, described above. For the flow sub-problem, we use the Equation-Of-State module No. 8 (EOS 8) of TOUGH2/iTOUGH2. This module accounts for three components (air, water, oil) and three phases (gas, aqueous and non-aqueous phase liquid [NAPL]). Mass flow occurs by advection, and heat flow occurs by conduction and convection. In order to simplify the physics involved, no volatilization or dissolution of the oil component is accounted for, resulting in a “dead-oil” approximation (i.e., the oil component is only present in the NAPL phase, which is solely composed of oil). This simplification is thought to be adequate in the current study because the main focus is on two-way coupled flow and geomechanics processes in heavy oil reservoirs (i.e., low volatility hydrocarbons), and on the response of the reservoir rock to thermal effects. Nevertheless, a few enhancements have been introduced to EOS 8 (Blanco-Martín et al., 2015). Several three-phase relative permeability functions have been implemented (such as Parker’s and Stone’s I models [Parker et al., 1987; Stone, 1970]), because previous studies by Baker (1988) and Kumar and Do (1990) highlighted the relevance of relative permeability models and endpoint saturations to predict reservoir performance. Fig. 5 shows three ternary plots with gas, aqueous and NAPL isoperms (isocontours of relative

permeability) corresponding to Parker's model (Parker et al., 1987), with S_m=0.35 and n=100. Parameter n is given a high value to linearize this model and make it similar to the linear interpolation model, which was found to predict more accurately experimental residual oil saturation to steam in thermal stimulation (Kumar and Do, 1990). As Fig. 5c shows, parameter S_m is related to the saturation of the aqueous phase when the slope of the NAPL relative permeability changes.

(a)

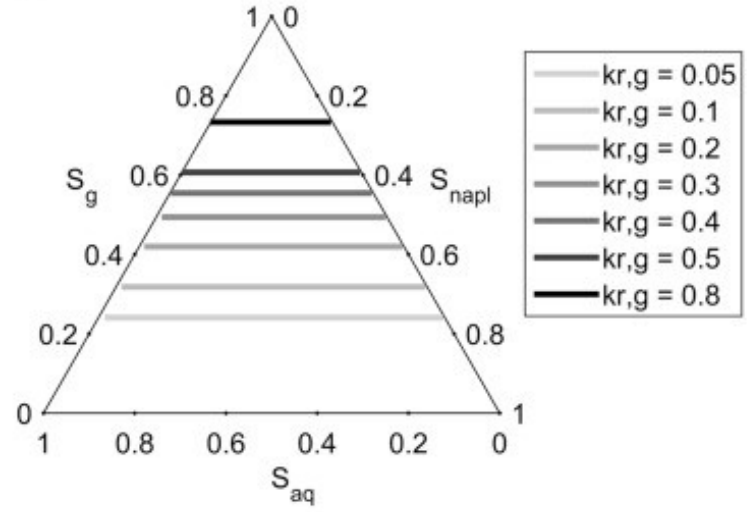
1
0
0.8
0.2
0.6
0.4
S_g
S_{napl}
0.4
0.6
0.2
0.8
0
1
1
0.8
0.6
0.4
0.2
0
S_{aq}
kr,g = 0.05
kr,g = 0.1
kr,g = 0.2
kr,g = 0.3
kr,g = 0.4
kr,g = 0.5
kr,g = 0.8

(b)

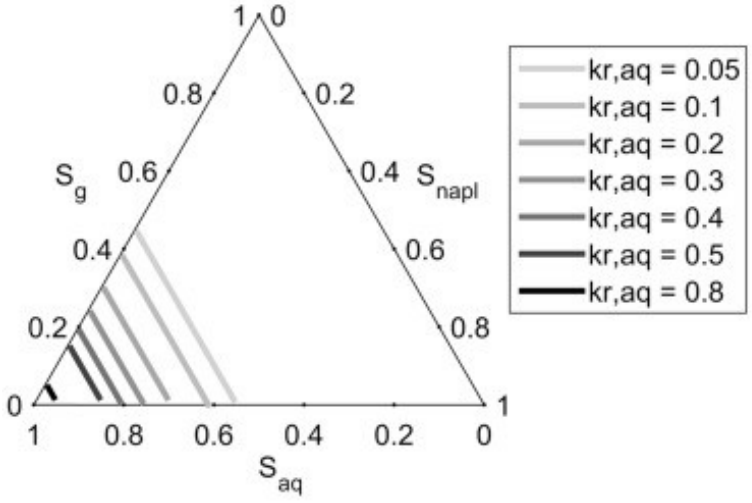
1
0
0.8
0.2
0.6
0.4
S_g
S_{napl}
0.4
0.6
0.2
0.8
0
1
1
0.8
0.6
0.4
0.2
0
S_{aq}
kr,aq = 0.05
kr,aq = 0.1
kr,aq = 0.2
kr,aq = 0.3
kr,aq = 0.4
kr,aq = 0.5
kr,aq = 0.8

(c)

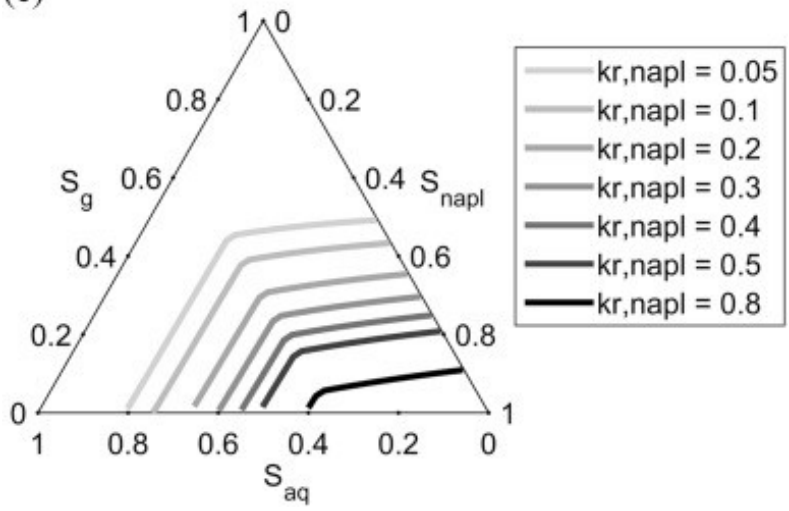
1
0
0.8
0.2
0.6
0.4
S_g
S_{napl}
0.4
0.6
0.2
0.8
0
1
1
0.8
0.6
0.4
0.2
0
S_{aq}
kr,napl = 0.05
kr,napl = 0.1
kr,napl = 0.2
kr,napl = 0.3
kr,napl = 0.4
kr,napl = 0.5
kr,napl = 0.8

1. Download high-res image (401KB)
2. Download full-size image

Fig. 5. Ternary relative permeability plots for diatomite showing: (a) gas phase isoperms; (b) aqueous phase isoperms; (c) NAPL phase isoperms. Parker's model has been calibrated to match data in Kumar and Do (1990).

Finally, we note that other enhancements to the standard EOS8 module are related to the implementation of a three-phase capillary pressure function (Parker et al., 1987, Pruess and Battistelli, 2002), and an empirical correlation to compute NAPL viscosity (Van Velzen et al., 1972). These enhancements have been introduced to model heavy oil diatomite reservoirs accounting for available data. Fig. 6 shows experimental and modeled water-oil capillary pressure for heavy oil diatomite, and Fig. 7 shows measured and modeled temperature-dependent viscosity of the heavy oil (Kumar and Beatty, 1995).

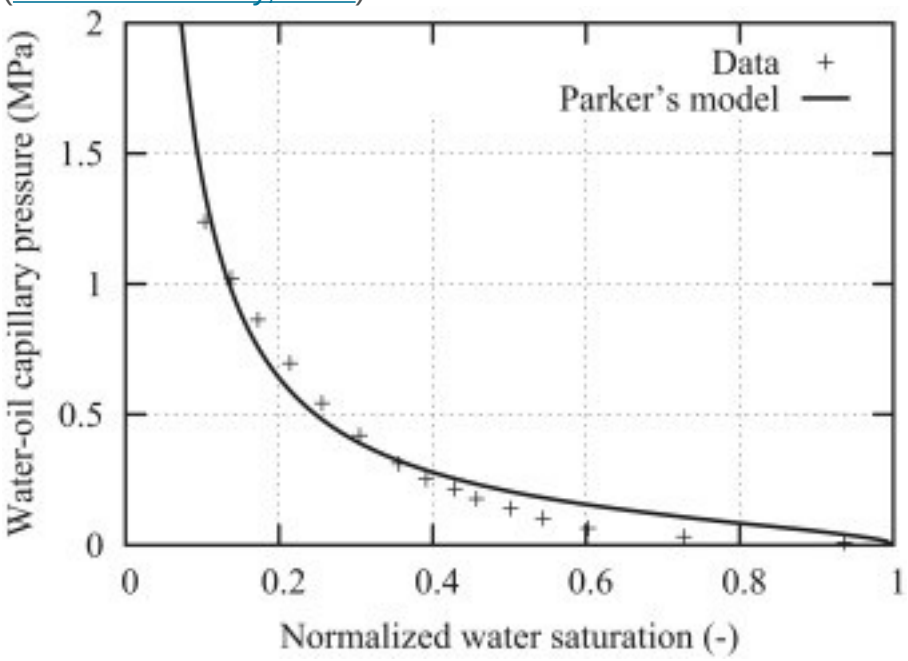

1. Download high-res image (159KB)
2. Download full-size image

Fig. 6. Experimental and fitted water-oil capillary pressure (Parker's model) for heavy oildiatomite (data from Kumar and Beatty (1995)).

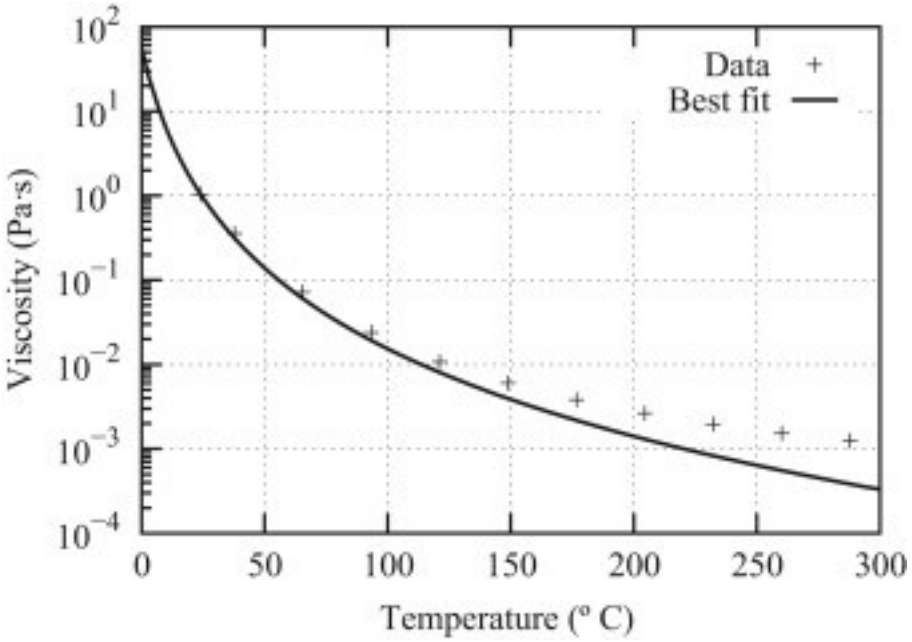

1. Download high-res image (154KB)
2. Download full-size image

Fig. 7. Experimental and fitted viscosity of heavy oil in diatomite. Data in Kumar and Beatty (1995) are modeled with an empirical equation by Van Velzen et al. (1972).

3. THM modeling of a symmetric well pattern

3.1. Model description

A generic, symmetric pattern of wells undergoing cyclic steaming is selected to investigate the importance of thermal weakening on the mechanical response of diatomite and induced ground surface displacement. Initially, the pattern consists of four wells located at the corners of a 50 m wide square. After a few years, a fifth well is added in the middle of the original pattern to increase recovery. This pattern, shown in Fig. 8a, is somewhat similar to reported practice in heavy oildiatomite fields (Ambastha et al., 2001, Fong et al., 2001).

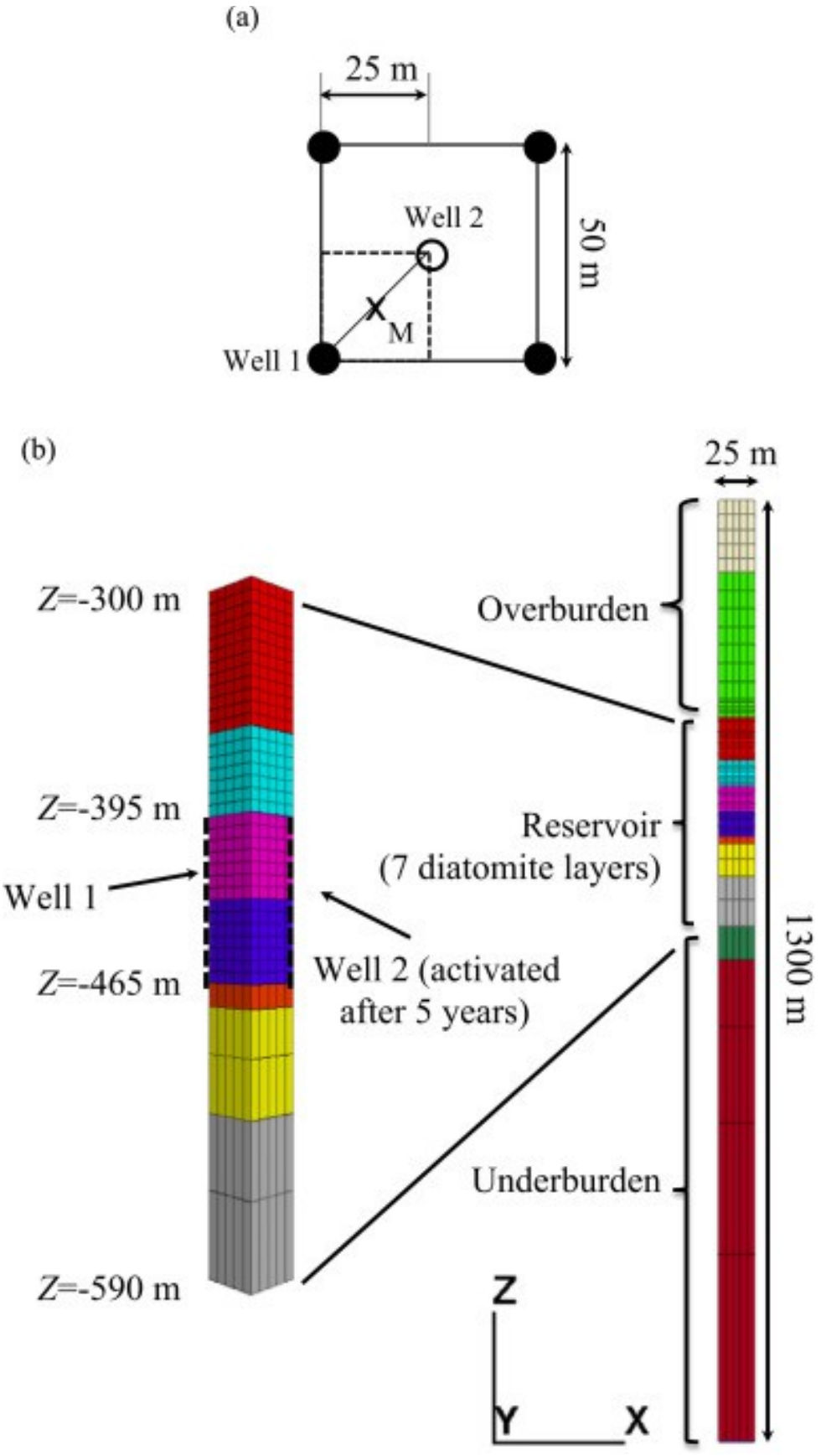
(a)
25 m
Well 2
50 m
M
Well 1
(b)
25 m
Z=-300 m
Overburden
Z=-395 m
Reservoir
(7 diatomite layers)
Well 1
Z=-465 m
Well 2 (activated
after 5 years)
1300 m
Underburden
Z=-590 m
Z
Y
X

1. Download high-res image (411KB)
2. Download full-size image

Fig. 8. (a) map-view of symmetric well pattern studied, including observation locations (*Well 1*, *Well 2*, *M*); (b) model geometry, including enlarged view of the reservoir.

The model extends vertically from the ground surface to a depth of 1300 m. The reservoir extends from Z=−300 m to Z=−590 m. The wells are open along a 70 m-long section starting at Z=−395 m. The overburden consists of 100 m of alluvium (vadose zone) and 200 m of oil-rich sands. The underburden is composed of upper and lower porcellanite (opal-CT, with reduced porosity – a layer typically not produced). Fig. 8b shows an overall view of the model geometry and an enlarged view of the reservoir, including the open well section.

The diatomite reservoir is initially in two-phase conditions (aqueous and NAPL). Porosity decreases with depth along the reservoir, and so do permeability and initial oil saturation (Miller and McPherson, 1992). The oil-rich sands and the underburden layers are also in two-phase conditions. To reflect anisotropy, vertical and horizontal permeabilities are different. Table 1 lists the thickness of each material group as well as relevant flow properties. These properties have been adopted from data published for diatomite reservoirs (Ambastha et al., 2001, Crawford et al., 2006, DOGGR, 1998, Fong et al., 2001, Kumar and Beatty, 1995, Kumar and Do, 1990). For all layers, Parker's functions for three-phase relative permeability and capillary pressure are used (Parker et al., 1987). We note that, in order to account for previous production activities (most of which likely involved fracturing), the initial permeability of the reservoir is increased by one order of magnitude; note also that permeability remains constant during the THM simulation. Finally, initial pore pressure and temperature for each layer are obtained from a steady-state simulation holding atmospheric conditions(P=0.1 MPa, T=18 °C) at the top boundary.

Table 1. Flow properties and initial conditions of each material group.

Material	Alluvium	Oil-rich sands	Reservoir	Upper Porcellanite	Lower Porcellanite
Thickness [m]	100	200	290	45	665
Initial phase partitioning (S_g,S_{aq},S_{napl}) [%]	(99,1,0)	(0,30,70)	(0,43,57)[a]	(0,18,82)	(0,18,82)
Grain density [kg m^{-3}]	2830	2650	2350	2455	2730
Initial porosity [%]	35	35	68[a]	45	45
Horizontal permeability, k_h [m^2]	$1.0\cdot10^{-13}$	$3.0\cdot10^{-12}$	$8.0\cdot10^{-14}$[a]	$3.2\cdot10^{-16}$	$3.2\cdot10^{-16}$
Permeability	100	2	2	1	1

Material	Alluvium	Oil-rich sands	Reservoir	Upper Porcellanite	Lower Porcellanite
ratio, k_h/k_v [dimensionless]					
Thermal conductivity [W m^{-1} K^{-1}]	3.1	1.1	0.9	1.1	1.1
Grain heat capacity [J kg^{-1} K^{-1}]	1000	1000	1500	2500	2500

a

Values decrease with depth following Miller and McPherson (1992).

As for geomechanics, the modified Cam-clay model with a temperature-dependent cap is applied to the reservoir rock. Since the focus here is on the behavior of the reservoir, we assume that the overburden and underburden behave elastically, with mechanical properties displayed in Table 2. The reservoir is sub-divided into seven layers featuring different mechanical properties. These properties are adopted from available literature on diatomite reservoirs (in particular, Crawford et al., 2006; Fossum and Fredrich, 2000, Fossum. and Fredrich, 1998; Fredrich et al., 2000; Hansen et al., 1995; Minkoff et al., 2004). Table 3 lists relevant mechanical properties for each diatomite layer (the initial specific volume is computed from porosity using Eq. (2), λ is calculated using Eq. (8), v_λ is calculated from Eqs. (5), (6) and line intersections, and $p_1=p_0$). Moreover, since significant damage due to past production may have occurred (Crawford et al., 2006), we assume that the initial stress field within the diatomite lies on the yield surface (the consolidation pressure listed in Table 3 is computed accordingly).

Table 2. Mechanical properties of the overburden and the underburden.

Material	Alluvium	Oil-rich sands	Upper Porcellanite	Lower Porcellanite
Bulk modulus, *K* [MPa]	203	250	566	1970
Shear modulus, *G* [MPa]	100	120	479	962

Table 3. Mechanical properties of the reservoir layers.

Material	Layer 1	Layer 2	Layer 3	Layer 4	Layer 5	Layer 6	Layer 7
Thickness [m]	60	35	35	35	10	45	70
Bulk modulus, *K* [MPa][a]	300	283	275	267	260	256	248
Poisson's ratio, ν [dimensionless]	0.27	0.27	0.27	0.27	0.27	0.27	0.27
κ [dimensionless]	0.035	0.035	0.035	0.035	0.035	0.035	0.035
***M* [dimensionless]**	1.732	1.155	1.715	3.333	3.711	2.078	1.367
$p_{c,0}$ [MPa][b]	4.18	5.88	4.93	4.30	4.42	5.15	6.92

a

at top of layer (values evolve following $K=pv/\kappa$).

b

calculated zone-by-zone from the stress state (see text).

The generalized field is operated as follows: for about five years, cyclic steaming is performed on the original four-well pattern (filled dots in Fig. 8a). Each cycle consists of 6 days of steam injection, 4 days of soaking and 22 days of production (total of 32 days/cycle). After 5.3 years (1920 days or 60 cycles), the center well (non-filled dot in Fig. 8a) comes into operation (infill drilling, see Fong et al. (2001)) and is synchronized with the original pattern. Ten and a half years of additional cyclic steaming (120 cycles) on the extended well pattern are then modeled. According to Ambastha et al. (2001), steam is injected at a rate of 500 STB/day/well cold water equivalent (0.92 kg/s/well). For a pressure of about 3 MPa and steam quality of 70%, the specific enthalpy of the injected fluid is 2.1 MJ/kg (T≈240 °C). Production occurs under self-flowing conditions, i.e., the wells are not actively pumped during this phase.

3.2. Results considering thermally induced diatomite compaction

Fig. 9 shows the pore pressure evolution during 15.8 years of cyclic steaming at three different depths: Z=−395, −430 and −465 m, corresponding, respectively, to the top, middle, and bottom of the wells perforation interval. The oscillations observed are due to the cycles: pore pressure increases during injection and decreases slightly during soaking and substantially during production. The pressure increase observed at 5–6 years is due to the activation of the center well. It should be noted that, for a given depth, the average pore pressure does not change noticeably over time. This is a major difference as compared to primary recovery methods, in which the pore pressure is depleted significantly.

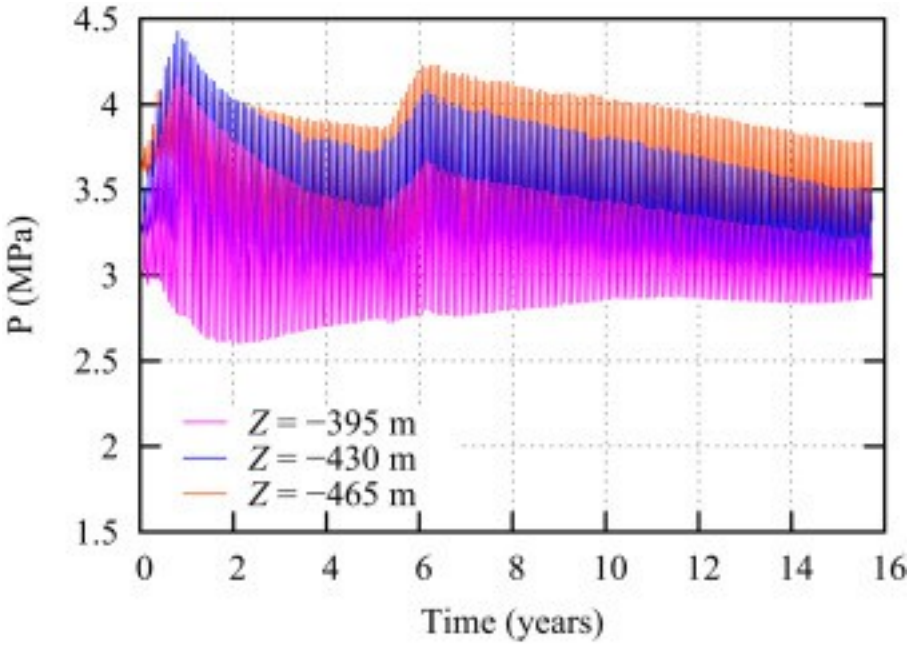

1. Download high-res image (459KB)
2. Download full-size image

Fig. 9. Evolution of pore pressure at three different depths in the reservoir (case with thermally induced diatomite compaction).

Fig. 10 displays the temperature evolution at the depths displayed in Fig. 9, but at three locations per depth, corresponding to *Well 1*, *Well 2* and *M* in Fig. 8a. Temperature increases initially in the area close to *Well 1*, and spreads horizontally. The lower part of the reservoir never reaches the same temperature as the upper part because the injected steam tends to travel up due to buoyancy. At the middle observation location (*M*), temperature increases smoothly at each depth displayed. As the second well is activated after 5.3 years, temperature increases at *Well 2* similarly as it did initially at *Well 1*. After 15.8 years, temperature at location *M* is close to that at *Well 1* and *Well 2* (in particular at shallower depths), reflecting some well interference.

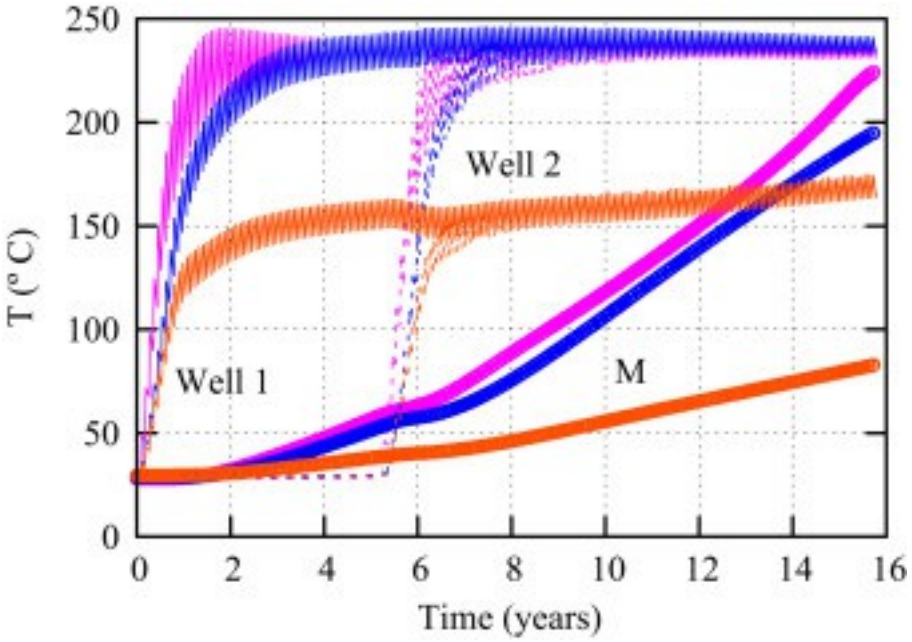

1. Download high-res image (444KB)
2. Download full-size image

Fig. 10. Evolution of temperature at six different locations in the reservoir (case with thermally induced diatomite compaction). Each depth is represented by the same color as in Fig. 9.

Progressive heating of the reservoir reduces viscosity of the oil, allowing it to flow to the wells. Fig. 11 displays the evolution of NAPL saturation (i.e., volume of NAPL phase divided by pore volume) at the locations displayed in Fig. 10. Initially, injected steam condenses and the NAPL phase is pushed away from the well. After a few cycles, as the system is gradually heated, oil viscosity reduces and the NAPL phase flows to the well. Fig. 11, Fig. 10 show a strong inverse correlation between oil saturation and temperature, with the hottest locations showing the highest oil recovery. According to Fig. 5c, for S_{napl}≈20% the relative permeability of the oil phase is quite low, which results in low mobility. At location *M*, the maximum oil saturation change after 15.8 years of cyclic steaming does not exceed 15%, while it exceeds 25% close to *Well 1* and *Well 2*, as a result of temperature contrast at these locations.

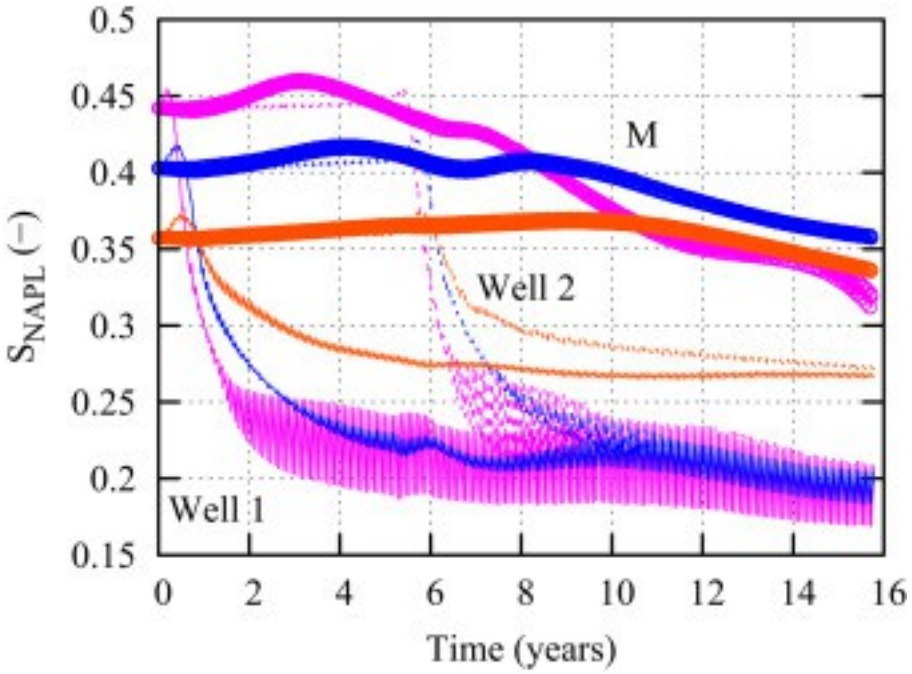

1. Download high-res image (464KB)
2. Download full-size image

Fig. 11. Evolution of NAPL saturation at the locations displayed in Fig. 10 (case with thermally induced diatomite compaction).

From a mechanical point of view, the stress state within the reservoir is affected by pore pressure, temperature and mass changes (Coussy, 2004). Due to the cycles, the mean effective stress, p, decreases during injection (because the pore pressure increases) and increases during production (pore pressure reduction). An increase in mean effective stress could bring the stress state to the yield envelope (compaction domain, $p>p_c/2$); however, since the average pore pressure does not change much over time (only slight decrease, see Fig. 9), non-recoverable compaction due to pore pressure change is not a dominant mechanism in this case. On the other hand, as temperature increases progressively within the diatomite (see Fig. 10), parameter λ and the consolidation pressure (p_c) decrease according to the approach presented in Section 2.1, triggering a decrease in the size of the elastic domain, which in turn causes additional inelastic compaction. Fig. 12 shows the porosity change around locations *Well 1* and *Well 2* after 15.8 years of cyclic steaming. In TOUGH-FLAC, porosity is computed using the approach described in Kim et al. (2012) for coupled flow and geomechanics. On average, porosity has been reduced by 5% in the reservoir. Owing to reservoir compaction, the ground surface subsides as shown in Fig. 13 (note that given the small lateral extent of the model, subsidenceis uniform). After 15.8 years,

almost 2 m of subsidence are predicted; this result is consistent with the average porosity reduction within the reservoir.

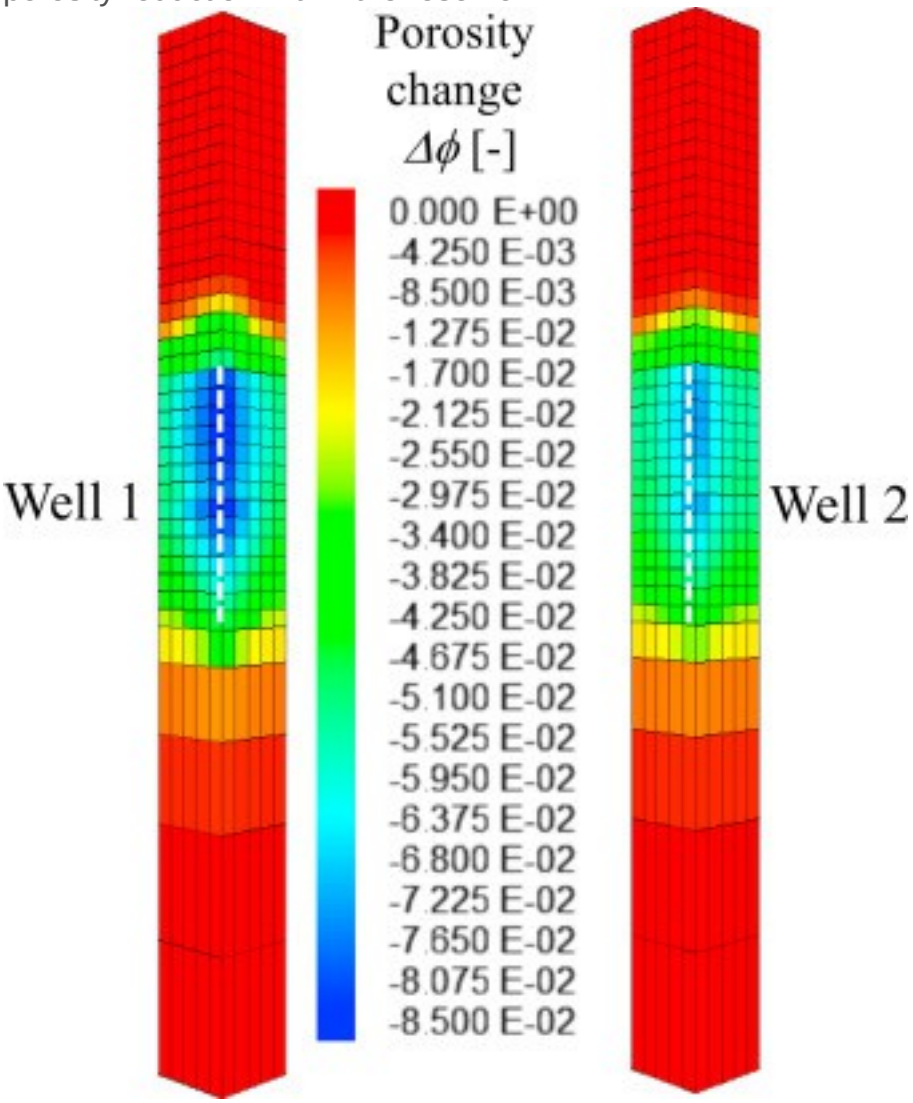

1. Download high-res image (459KB)
2. Download full-size image

Fig. 12. Porosity contour within the reservoir, around locations corresponding to *Well 1* and *Well 2* (case with thermally induced diatomite compaction).

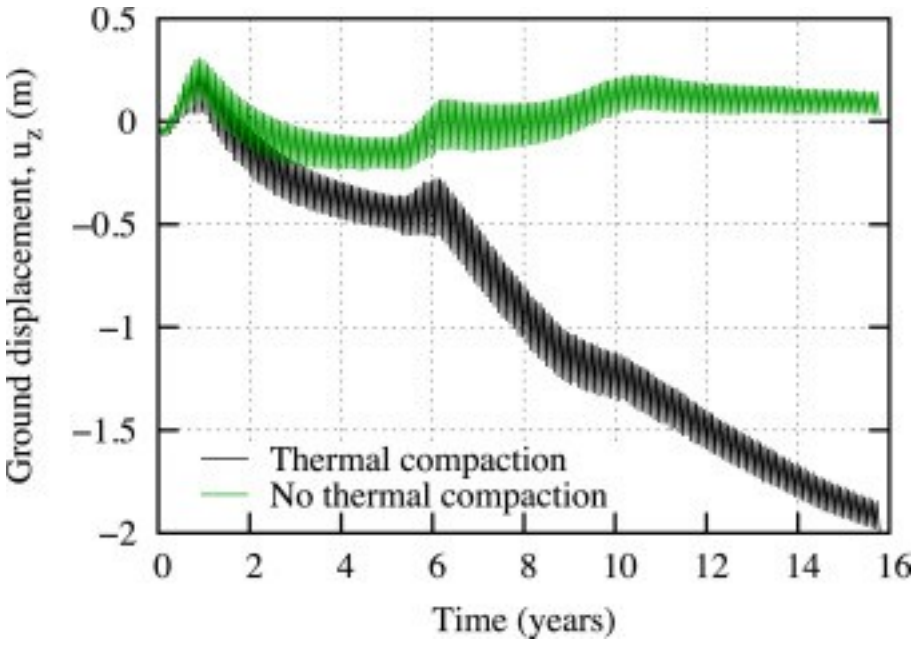

1. Download high-res image (273KB)
2. Download full-size image

Fig. 13. Evolution of subsidence when thermally induced compaction is included or disregarded.

3.3. Results disregarding thermally induced diatomite compaction

In order to quantify the importance of thermal effects on the response of the reservoir rock, we have performed a simulation equivalent to the one described in the previous section, but without a provision for thermally induced compaction in the modified Cam-clay model. In this case, plastic compaction is driven mostly by changes in pore pressure over time. The pore pressure, temperature and NAPL saturation at the observation points are displayed in Fig. 14, Fig. 15, Fig. 16, respectively; they are very similar to those obtained when thermally induced compaction is considered (see Fig. 9, Fig. 10, Fig. 11).

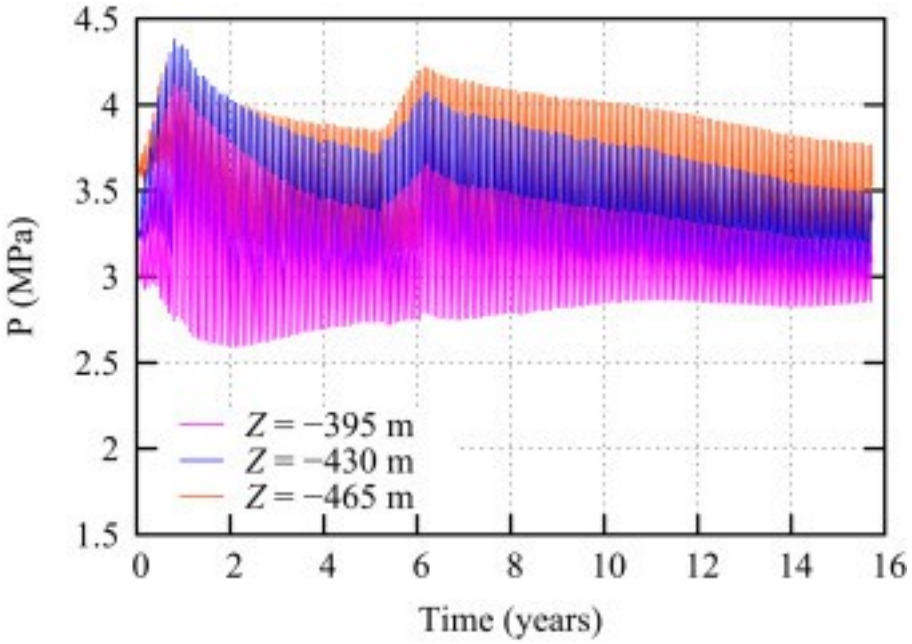

1. Download high-res image (467KB)
2. Download full-size image

Fig. 14. Evolution of pore pressure at three different depths in the reservoir (case without thermally induced diatomite compaction).

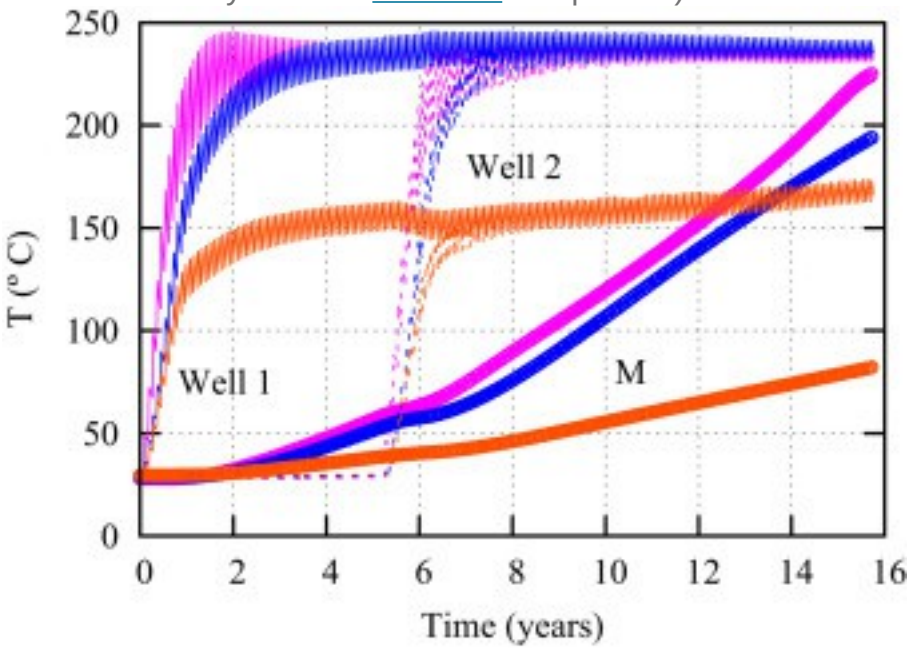

1. Download high-res image (437KB)
2. Download full-size image

Fig. 15. Evolution of temperature at six different locations in the reservoir (case without thermally induced diatomite compaction). Each depth is represented by the same color as in Fig. 14.

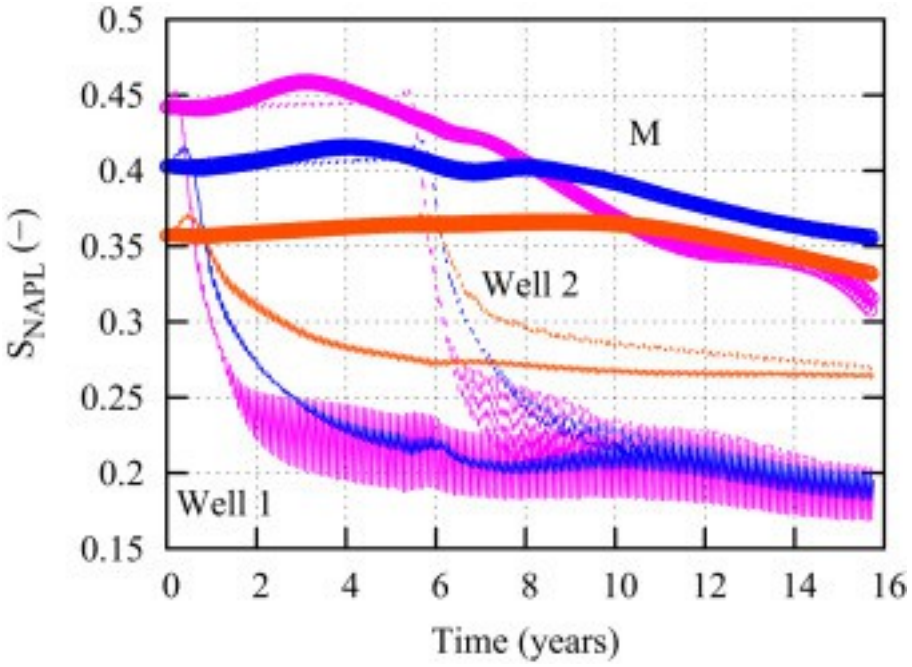

1. Download high-res image (449KB)
2. Download full-size image

Fig. 16. Evolution of NAPL saturation at the locations displayed in Fig. 15 (case without thermally induced diatomite compaction).

However, as Fig. 17 shows, porosity changes within the reservoir after 15.8 years of cyclic steaming are approximately 50% lower than the changes predicted when thermally induced compaction is accounted for. The amount of non-produced fluids (saturation×porosity) is therefore larger in the current case. The similar trends in pore pressure observed in Fig. 9, Fig. 14 are due to a higher mass production (oil and water) when thermally induced compaction is taken into account.

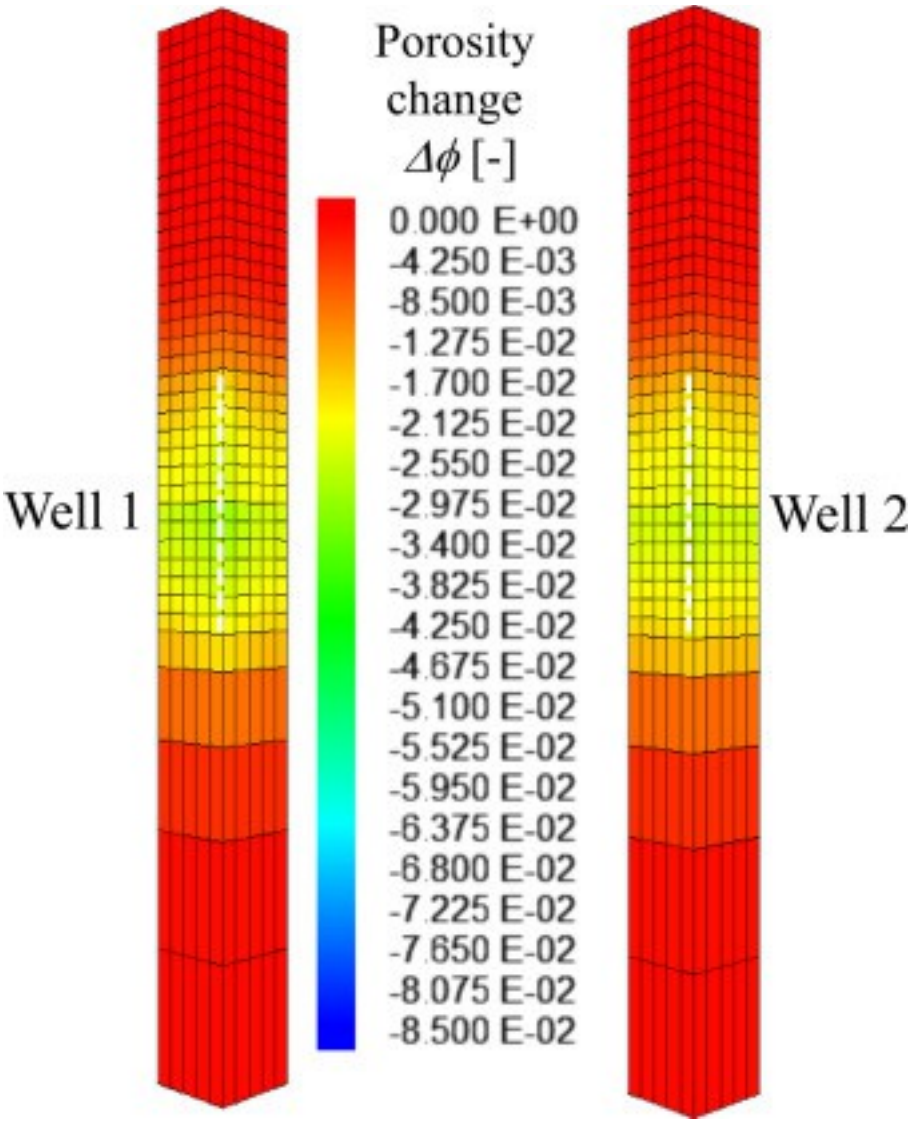

1. Download high-res image (462KB)
2. Download full-size image

Fig. 17. Porosity contour within the reservoir, around locations corresponding to *Well 1* and *Well 2* (case without thermally induced diatomite compaction).

4. Discussion

The consolidation pressure over time predicted by the two simulations is shown in Fig. 18, at Z=−465 m for locations *Well 1*, *Well 2* and *M*. Clearly, temperature has a dominant effect on the weakening of diatomite (reduction of p_c), and therefore it potentially induces additional inelastic strain. Note that the change in trend in $p_c$when thermal weakening is considered is due to the inflection point observed experimentally at approximately 102 °C (see Fig. 1b); indeed, Fig. 10 indicates a temperature of about 102 °C after 250 days at location *Well 1*, and after 2160 days (about 6 years) at

location *Well 2*. On the other hand, at location *M*temperature increases progressively but does not reach 102 °C after 15.8 years; consequently, the consolidation pressure decreases smoothly over time at this location. We note that when thermally induced compaction is not considered (and when thermal effects are less important [*T*>102 °C]), the consolidation pressure increases slightly (hardening); this increase is due to plastic compaction that occurs progressively over time as the pore pressure decreases (see Fig. 9, Fig. 14).

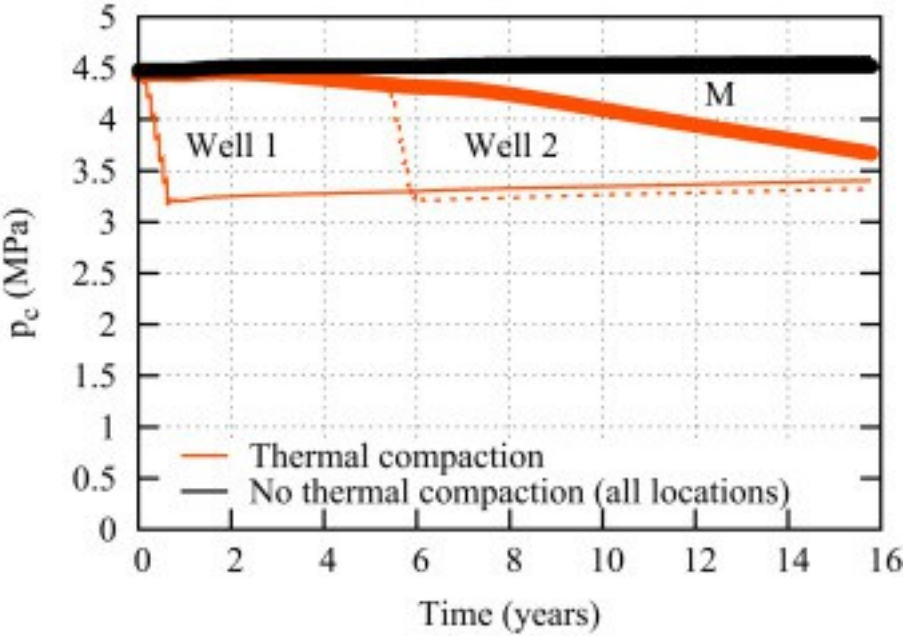

1. Download high-res image (223KB)
2. Download full-size image

Fig. 18. Consolidation pressure over time at locations *Well 1*, *Well 2* and *M* for *Z*=−465 m, when thermally induced compaction is included or disregarded.

The stress path in the *p*−*q* plane predicted by the two simulations for location *Well 1* at *Z*=−465 m is shown in Fig. 19. When thermally induced compaction is considered, the reduction in the cap size (reduction of p_c) as temperature increases triggers a larger change in effective stresses. Beyond 102 °C, once the temperature effect becomes less important, progressive hardening occurs (increase of p_c). On the other hand, when thermally induced compaction is disregarded, progressive hardening occurs from the beginning of the simulation.

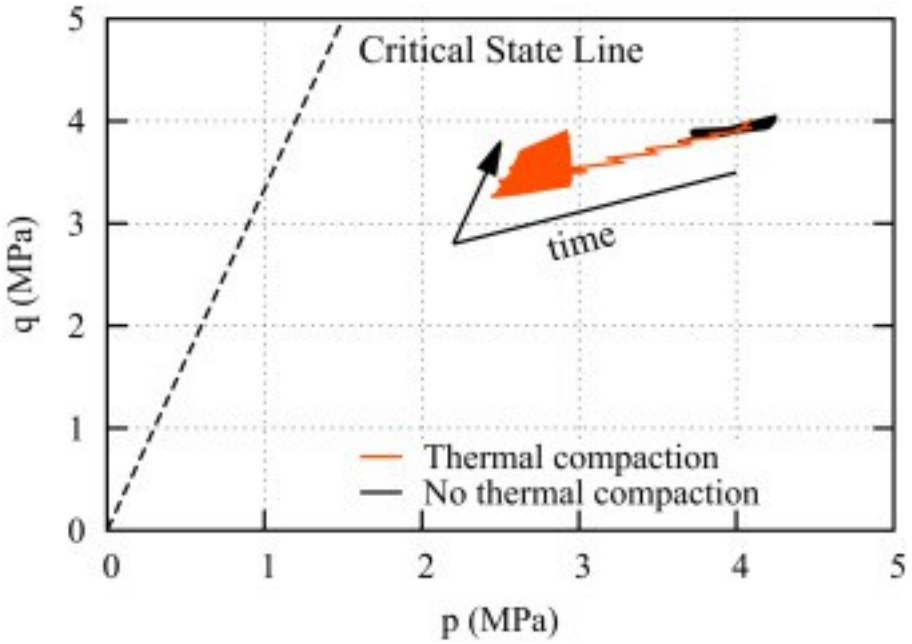

1. Download high-res image (166KB)
2. Download full-size image

Fig. 19. Stress path at location *Well 1* for Z=−465 m, when thermally induced compaction is included or disregarded.

Additional compaction due to thermal weakening explains the greater porosityreduction shown in Fig. 12. Due to the differences in reservoir response, the ground surface displacement computed by the two simulations is also quite different (see Fig. 13). While almost no net subsidence is predicted when thermally induced compaction is neglected, about 2 m of subsidence are obtained when thermal effects on diatomite are considered.

Finally, we highlight that the adopted model geometry is suitable to investigate the behavior of the reservoir rock under transient hydraulic, thermal and mechanical conditions, and also to study local effects around wells; however, the simplicity and limited lateral extent of the model prevent its use to investigate shear processes on a scale large enough to create well damage or failure. Moreover, while the current investigation focuses on the reservoir response, well damage — although often triggered by the reservoir response — likely happens in the overburden (Fredrich et al., 2000). Therefore, the work presented here is an initial step aimed at understanding relevant mechanisms in diatomite reservoirs, prior to addressing well shear failure and associated reservoir macro-scale movements, which will be investigated in a second step.

5. Conclusions

Shallow, heavy oil diatomite reservoirs produced using cyclic steaming are often associated with significant subsidence. In this study, we performed coupled THM modeling to investigate whether thermally induced compaction of the reservoir rock could be a key factor to explain ground surface subsidence. Thermal effects in diatomite could be of particular importance as the mechanism responsible for reservoir compaction and related subsidence in cases where the reservoir pore pressure is not allowed to deplete noticeably.

Published laboratory-scale studies have shown that, under increased temperatures, diatomite (amorphous silica) undergoes dissolution/precipitation and mineralogical transformations that result in non-reversible reduction of porosity, as well as in the modification of other flow and mechanical properties (loss of mechanical integrity).

In order to model these observations, we have introduced temperature dependence into the plastic response of the modified Cam-clay model. In particular, as temperature increases, the size of the elastic domain decreases, thereby reducing the threshold for non-reversible deformation. Parameters needed to model thermally induced compaction of diatomite are calibrated from available experimental data at laboratory-scale. We note that dissolution/precipitation and mineralogical transformations are not modeled explicitly, but rather the overall behavior is parameterized to fit the observed macroscopic response.

This new approach is then applied to model a symmetric pattern of wells in a diatomite reservoir produced using cyclic steaming. With the aim of determining the importance of thermally induced compaction on the mechanical response of the reservoir rock and on induced subsidence, we compare results from two THM simulations that use, respectively, the standard or the temperature-enhanced modified Cam-clay model. Although the scenario studied is generic and simplified, the results show that thermally induced diatomite compaction can potentially induce significant inelastic pore volume reduction and substantial subsidence.

These results suggest that, at a larger scale, thermally induced compaction may play an important role in massive well shear failure, particularly if linked with differential movements in the overburden (caused for instance by contrasts in mechanical properties). This will be addressed in a subsequent phase of research.

Acknowledgments

Support for this work was provided in part by Lawrence Berkeley National Laboratory under Department of Energy Contract No. DE-AC02-05CH11231.

References

Ambastha et al., 2001

Ambastha, A.K., Kumar, M., Skow, L.A., Evola, G.M., 2001. Evaluation of Cyclic Steam Operations at Cymric 1A Diatomite. SPE Annual Conference, Sept. 30-Oct.3 (SPE 71500).

Baker, 1988

Baker, L.E., 1988. Three-Phase Relative Permeability Correlations. SPE/DOE Symp., April 17–20 (SPE/DOE 17369).

Blanco-Martín et al., 2015

Blanco-Martín, L., Rutqvist, J., Doughty, C.A., Zhang, Y., Finsterle, S., Oldenburg, C.M., 2015. iTOUGH2-FLAC Modeling of Thermal-Hydraulic-Mechanical Processes Related to Steam-Assisted Heavy Oil Recovery from Diatomite. Proc. TOUGH Symp.

Bruno, 1990

Bruno, M.S., 1990. Subsidence-Induced Well Failure. SPE Calif. Regional Meeting, April 4–6 (SPE 20058).

Coussy, 2004

O. Coussy**Poromechanics**

(1st ed.), John Wiley and Sons, Chichester, UK (2004)

Crawford et al., 2006

Crawford, B.R., Searles, K.H., Hsu, S.-Y., Reese, W.L., Urdaneta, A.H., Carnahan, B.D., Martin, J.W., 2006. Plastic Compaction in Diatomite: In Situ Stress versus Temperature Effects. 41st ARMA Symp., June 17–21 (ARMA 06–1122).

DeRouffignac et al., 1995

DeRouffignac E.P., Bondor, P.L., Karanikas, J.M., Hara, S.K., 1995. Subsidence and Well Failure in the South Belridge Diatomite Field. SPE Western Regional Meeting, March 8–10 (SPE 29626).

Dietrich, 2010

Dietrich, J.K., 2010. The Displacement of Heavy Oil From Diatomite Using Hot Water and Steam. SPE Improved Oil Recovery Symp., April 24–28 (SPE 129705).

Dietrich and Scott, 2007

Dietrich, J.K., Scott, J.D., 2007. Modeling Thermally Induced Compaction in Diatomite. SPE J. 12(1):130-144 (SPE 97849). 10.2118/97849-PA

DOGGR, 1998

DOGGR, California Department of Conservation Division of Oil, Gas and Geothermal Resources, 1998. California Oil and Gas Fields, Volume I, Central California, Publication No. TR11, Sacramento, Calif.

Doherty, 2008

Doherty, J., 2008. PEST: Model-Independent Parameter Estimation, Watermark Numerical Computing, Brisbane.

Finsterle et al., 2016

S. Finsterle, M. Commer, J. Edmiston, Y. Jung, M.B. Kowalsky, G.S.H. Pau, H.Wainwright, Y. Zhangi**TOUGH2: a simulation-optimization framework for analyzing multiphysics subsurface systems**

Comput. Geosci. (2016)

(in preparation)

Finsterle, 2015

S. Finsterle**Enhancements to the TOUGH2 Simulator Implemented in iTOUGH2**

Report LBNL-7016E

Lawrence Berkeley National Laboratory, Berkeley, Calif (2015)

Finsterle_and_Zhang,_2011

S. Finsterle, Y. Zhang**Solving iTOUGH2 simulation and optimization problems using the PEST protocol**

Environ. Model. Softw., 26 (7) (2011), pp. 959-968, 10.1016/j.envsoft.2011.02.008
ArticleDownload PDFView Record in Scopus

Finsterle, 2004

S. Finsterle**Multiphase inverse modeling: review and iTOUGH2 applications**
Vadose Zone J., 3 (2004), pp. 747-762, 10.2113/3.3.747
CrossRefView Record in Scopus

Fong et al., 2001

Fong, W.S., Lederhos, L., Skow, L.A., Evola, G.M., Choi, J., 2001.Analysis of a Successful Cyclic Steam Process at Cymric Field, California. In: Proceedings of the SPE International Thermal Operations and Heavy Oil Symp., March 12-14 (SPE 69702)

Fossum and Fre 2000

A.F. Fossum, J.T. Fredrich**Constitutive Models for the Etchegoin Sands, Belridge Diatomite, and Overburden Formations at the Lost Hills Oil Field, California**
Report SAND2000-0827
Sandia National Laboratories, Albuquerque, New Mexico (2000)

Fossum. and Fre

A.F. Fossum, J.T. Fredrich**Estimation of Constitutive Parameters for the Belridge Diatomite, South Belridge Diatomite Field**
(Report SAND)
Sandia National Laboratories, Albuquerque, New Mexico (1998), pp. 98-1407
View Record in Scopus

Fredrich et al., 2

J.T. Fredrich, J.G. Argüello, G.L. Deitrick, E.P. DeRouffignac**Geomechanical modeling of reservoir compaction, surface subsidence and casing damage at the Belridge Diatomite Field**
SPE Reserv. Eval. Eng., 3 (4) (2000)
(SPE 65354)

Fredrich et al., 1

Fredrich, J.T., Argüello, J.G., Thorne, B.J., Wawersik, W.R., Deitrick, G.L., DeRouffignac, E.P., Myer, L.R., Bruno, M.S., 1996. Three-dimensional geomechanical simulation of reservoir compaction and implications for well failures in the Belridge Diatomite. In: Proceedings of the SPE Annual Technical Conference and Exhibition, Denver, Oct. 6–9 (SPE 36698).

Hamilton et al., 1

Hamilton, J.M., Maller, A.V., Prints, M.D., 1992. Subsidence-induced shear failures above oil and gas reservoirs. In: Proceedings of the33rd US Symp. on Rock Mechanics (paper 263).

Hansen et al., 19

Hansen, K.S., Prats, M., Chan, C.K., 1995. Modeling of reservoir compaction and surface subsidence at South Belridge. In: Proceedings of theSPE Western Regional Meeting, Anchorage, May 26–28 (SPE 26074).

Hascakir and Ko

Hascakir, B., Kovscek, A.R., 2010. Reservoir simulation of cyclic steam injection including the effects of temperature induced wettability alteration. In: Proceedings of the SPE Western Regional Meeting, May 27–29 (SPE 132608).

Hilbert et al., 199

Hilbert, L.B., Gwinn, R.L., Moroney, T.A., Deitrick, G.L., 1999. Field-Scale and Wellbore Modeling of Compaction-Induced Casing Failures. SPE Drill. & Completion, 14(2) (SPE 56863)

Hilbert et al., 199

Hilbert, L.B. Jr., Fredrich, J.T., Bruno, M.S., Deitrick, G.L., DeRouffignac, E.P., 1996. Two-Dimensional Nonlinear Finite Element Analysis of Well Damage due to Reservoir Compaction, Well-to-Well Interactions, and Localization on Weak Layers. 2nd North American Rock Mechanics Symp., June 19–21 (ARMA-96-1863)

Ilderton et al., 19

Ilderton, D.C., Patzek, T.W., Rector, J.W., Vinegar, H.J., 1994. Passive Imaging of Hydrofracture in South Belridge Diatomite. In: Proceedings of the SPE Annual Technical Conference and Exhibition, Sept. 25–28 (SPE 28383).

Itasca Consultin

Itasca Consulting Group, 2012. FLAC3D (Fast Lagrangian Analysis of Continua in 3D) Version 5.0 – User's Guide, Minneapolis, MN.

Koh et al., 1996

Koh, C.J., Dagenais, P.C., Larson, D.C., Murer, A.S., 1996. Permeability Damage in Diatomite due to In-Situ Silica Dissolution/Precipitation.SPE/DOE Improved Oil Recovery Symp., Tulsa, April 21–24 (SPE 35394)

Kim et al., 2012

J. Kim, E.L. Sonnenthal, J. Rutqvist**Formulation and sequential numerical algorithms of coupled fluid/heat flow and geomechanics for multiple porosity materials**
Int. J. Numer. Methods Eng., 92 (5) (2012), pp. 425-456, 10.1002/nme.4340
CrossRefView Record in Scopus

Kumar and Beat

Kumar, M., Beatty, F.D., 1995. Cyclic Steaming in Heavy Oil Diatomite. SPE Western Regional Meeting, March 8–10 (SPE 29623).

Kumar and Do, 1

Kumar, M. Do, T.N., 1990. Effects of endpoint saturations and relative permeability models on predicted steamflood performance. In: Proceedings of the SPE/DOE 7th Symp., April 22–25 (SPE/DOE 20202).

Miller and McPh

Miller, D.D., McPherson, J.G., 1992. South Belridge Field –U.S.A. San Joaquin Basin, California. In: Foster, N.H., Beaumont, E.A.,AAPG Treatise of Petroleum Geology, Atlas of Oil and Gas Fields, Structural Traps VII, pp. 221–244.

Minkoff et al., 20

S.E. Minkoff, C.M. Stone, S. Bryant, M. Peszynska**Coupled geomechanics and flow simulation for time-lapse seismic modeling**
Geophysics, 69 (1) (2004), pp. 200-211, 10.1190/1.1649388
CrossRefView Record in Scopus

Parker et al., 198

J.C. Parker, R.J. Lenhard, T. Kuppusamy**A parametric model for constitutive properties governing multiphase flow in Porous Media**
Water Resour. Res., 23 (4) (1987), pp. 618-624, 10.1029/WR023i004p00618
CrossRefView Record in Scopus

Pruess and Batti

K. Pruess, A. Battistelli**TMVOC, A Numerical Simulator for Three-Phase Non-isothermal Flows of Multicomponent Hydrocarbon Mixtures in Saturated-Unsaturated Heterogeneous Media, Report LBNL-49375**
Lawrence Berkeley National Laboratory, Berkeley, Calif (2002)

Pruess et al., 20

K. Pruess, C.M. Oldenburg, G. Moridis**TOUGH2 User's Guide, Version 2.1, Report LBNL-43134 Rev.**
Lawrence Berkeley National Laboratory, Berkeley, Calif (2012)

Roscoe and Burl

K.H. Roscoe, J.B. Burland**On the generalised stress–strain behavior of 'Wet Clay'**
J. Heyman, F.A. Leckie (Eds.), Engineering Plasticity, Cambridge University Press, Cambridge (1968), pp. 535-609
View Record in Scopus

Rutqvist, 2011

J. Rutqvist**Status of the TOUGH-FLAC simulator and recent applications related to coupled fluid flow and crustal deformations**
Comput. Geosci., 37 (2011), pp. 739-750, 10.1016/j.cageo.2010.08.006
ArticleDownload PDFView Record in Scopus

Rutqvist et al., 2

J. Rutqvist, Y.S. Wu, C.F. Tsang, G. Bodvarsson**A modeling approach for analysis of coupled multiphase fluid flow, heat transfer, and deformation in fractured porous rock**
Int. J. Rock. Mech. Min. Sci., 39 (2002), pp. 429-442, 10.1016/S1365-1609(02)00022-9
ArticleDownload PDFView Record in Scopus

Schofield and W

A.N. Schofield, C.P. Wroth**Critical State Soil Mechanics**

McGraw-Hill, London (1968)
ISBN 978–0641940484

Stone, 1970

H.L. Stone**Probability model for estimating three-phase relative permeability**
Trans. SPE AIME, 249 (1970), pp. 214-218, 10.2118/2116-PA
CrossRefView Record in Scopus

Van Velzen et al.

D. Van Velzen, R.L. Cardozo, H. Langenkamp**A liquid viscosity-temperature-chemical constitutive relation for organic compounds**
Ind. Eng. Chem. Fund., 11 (1) (1972), pp. 20-25
CrossRefView Record in Scopus

Wood, 1991

D.M. Wood**Soil Behaviour and Critical State Soil Mechanics**
Cambridge University Press, Cambridge (1991), 10.1017/CBO9781139878272

Yudovich and Mo

Yudovich, A., Morgan, D.R., 1989. Casing deformation in Ekofisk. JPT (paper 729).